THE ASTROPHYSICAL JOURNAL, 543:535–544, 2000 November 10


# GAMMA-LOUD QUASARS: A VIEW WITH *BeppoSAX*

F. TAVECCHIO,[1] L. MARASCHI,[1] G. GHISELLINI,[2] A. CELOTTI,[3] L. CHIAPPETTI,[4] A. COMASTRI,[5] G. FOSSATI,[6] P. GRANDI,[7] E. PIAN,[8] G. TAGLIAFERRI,[2] A. TREVES,[9] C. M. RAITERI,[10] R. SAMBRUNA,[11] AND M. VILLATA[10]

*Received 2000 February 23; accepted 2000 June 13*

## ABSTRACT

We present *BeppoSAX* observations of three $\gamma$-ray–emitting quasars, namely, 0836+710, 1510−089, and 2230+114. The three objects have been detected up to $\sim$100 keV showing extremely flat power-law spectra above 2 keV (energy index $\alpha_{2-10} = 0.3$–$0.5$). The soft X-ray spectrum of 0836+710 implies either an absorption column density higher than the Galactic one or an intrinsically very hard slope ($\alpha_{0.1-1} = -0.2$) below 1 keV. 1510−089 shows a soft excess, with the low-energy spectrum steeper ($\alpha_{0.1-1} = 1.6$) than the high-energy power law. The results are discussed in the framework of current inverse Compton models for the high-energy emission of flat-spectrum radio quasars and are used to estimate the physical quantities in the jet-emitting region and to shed light on the energy transport mechanisms in jets. Finally we discuss the estimates of the jet luminosity in the context of the Blandford & Znajek mechanism for jet production.

*Subject headings:* galaxies: individual (0836+710, 1510−089, 2230+114) — quasars: general — radiation mechanisms: nonthermal — X-rays: general

## 1. INTRODUCTION

Since the EGRET detection of about 60 blazars (BL Lac objects and flat-spectrum radio quasars [FSRQs]) in $\gamma$-rays (Mukherjee et al. 1997), the study of this class of objects has received renewed interest. A large fraction of the total power is in fact emitted in the $\gamma$-ray band, which is therefore crucial to testing different radiation models.

The bright $\gamma$-ray emission requires relativistic boosting (e.g., Dondi & Ghisellini 1995), confirming that the emission of blazars originates in relativistic jets. The spectral energy distribution (SED) of all observed blazars from radio to $\gamma$-rays shows two broad peaks, believed to be produced by relativistic electrons in the jet via the synchrotron and inverse compton (IC) processes, respectively. It has been suggested that the locations of the synchrotron and IC peaks and the "$\gamma$-ray dominance" (i.e., the luminosity ratio of the second to the first peak) are related to the power of the source so that all blazars lie along a spectral sequence (Fossati et al. 1998; Ghisellini et al. 1998). FSRQs have synchrotron and IC peaks located at lower energies and are more $\gamma$-ray dominated than the less powerful BL Lac objects.

It is widely believed that the IC emission from FSRQs is dominated by the scattering between high-energy electrons and soft photons external to the jet (external Compton [EC]). The latter ones may be produced by the accretion disk itself and be scattered/reprocessed in the broad line region (BLR) (Dermer & Schlickeiser 1993; Sikora, Begelman, & Rees 1994). However, other sources of seed photons (e.g., the synchrotron photons themselves, synchrotron self-Compton [SSC]) could contribute in the soft–medium X-ray band. Contributions due to other components, such as direct synchrotron emission or the high-energy tail of the blue bump, are also possible in the soft X-ray band. In the simplest case of a single EC component, the flat X-ray spectrum of FSRQs represents the low-energy side of the IC peak and therefore is due to *low-energy electrons* scattering the externally produced photons. This spectral band gives then information on a part of the electron spectrum that, because of self-absorption, is not accessible in the low-frequency synchrotron component.

The unprecedentedly wide band of *BeppoSAX* (from 0.1 up to 100 keV) is optimal to study the connection between the X-ray and $\gamma$-ray continua and constrain and disentangle different emission components. For these reasons we started a program to observe the brightest $\gamma$-ray blazars. Here we report results for three of them, namely, 0836+710, 1510−089, and 2230+114. After a summary of previous observations for each source (§ 2), we present the analysis of the *BeppoSAX* data (§ 3). The implications are discussed in § 4 in the framework of the EC model for FSRQs. Conclusions are given in § 5.

## 2. THE OBSERVED OBJECTS

All sources have been repeatedly observed in $\gamma$-rays by EGRET showing a steep spectrum. Results are summarized in Table 1 together with previous X-ray measurements from *ROSAT* and *ASCA*. In the following we briefly describe the sources' characteristics most relevant for the present work.

[1] Osservatorio Astronomico di Brera, via Brera 28, 20121 Milano, Italy.
[2] Osservatorio Astronomico di Brera, via Bianchi 46, 23807 Merate, Italy.
[3] Scuola Internazionale Superiore di Studi Avanzati/International School for Advanced Studies, via Beirut 2-4, 34014 Trieste, Italy.
[4] Istituto di Fisica Cosmica/Consiglio Nazionale delle Ricerche, via Bassini 15, 20133, Milano, Italy.
[5] Osservatorio Astronomico di Bologna, via Ranzani 1, 40127, Bologna, Italy.
[6] Center for Astrophysics and Space Sciences, University of California, San Diego, CA 92093-0424.
[7] Istituto di Astrofisica Spaziale/Consiglio Nazionale delle Ricerche, via Fosso del Cavaliere, 00133 Roma, Italy.
[8] Istituto di Tecnologie e Studio delle Radiazioni Extraterrestri/Consiglio Nazionale delle Ricerche, via Gobetti 101, 40129 Bologna, Italy.
[9] Universita' dell'Insubria, via Lucini 3, 22100, Como, Italy.
[10] Osservatorio Astronomico di Torino, Strada Osservatorio 20, 10025, Pino Torinese (TO), Italy.
[11] Pennsylvania State University, 525 Davey Lab, State College, PA 16802.

TABLE 1

SUMMARY OF THE OBSERVATIONAL CHARACTERISTICS OF THE SOURCES ANALYZED IN THIS WORK

| | | | *ROSAT*[b] | | *ASCA*[c] | | EGRET[d] | |
|---|---|---|---|---|---|---|---|---|
| SOURCE | $z$ | $N_{H,\,gal}$[a] ($\times 10^{20}$ cm$^{-2}$) | $F_X$ ($\times 10^{-12}$ ergs cm$^{-2}$ s$^{-1}$) | $\alpha_X$ | $F_X$ ($\times 10^{-12}$ ergs cm$^{-2}$ s$^{-1}$) | $\alpha_X$ | $F_\gamma$ ($\times 10^{-8}$ photons cm$^{-2}$ s$^{-1}$) | $\alpha_\gamma$ |
| 0836+710..... | 2.172 | 2.78 | 8.6 | $0.5 \pm 0.1$ | 14.0 | $0.45 \pm 0.05$ | $10.2 \pm 1.8$ | $1.62 \pm 0.16$ |
| | ... | ... | 4.4 | $0.5 \pm 0.1$ | ... | ... | ... | ... |
| 1510−089..... | 0.361 | 7.88 | $6.15 \pm 0.93$ | $0.9 \pm 0.4$ | 8.6 | $0.30 \pm 0.06$ | $18.0 \pm 3.8$ | $1.47 \pm 0.21$ |
| 2230+114..... | 1.037 | 5.05 | $3.32 \pm 0.44$ | ... | $3.1 \pm 0.2$ | $0.6 \pm 0.1$ | $19.2 \pm 2.8$ | $1.45 \pm 0.14$ |

[a] Data are from Dickey & Lockman 1990 (0836+710), Lockman & Savage 1995 (1510−089), and Stark et al. 1992 (2230+710).

[b] *ROSAT* 0.1–2 keV flux and energy index, $F_\nu \propto \nu^{-\alpha}$. Data are from Cappi et al. 1997 (0836+710, two observations), Siebert et al. 1996, Comastri et al. 1997 (1510−089), and Brinkmann et al. 1994 (2230+114).

[c] *ASCA* 2–10 keV flux and energy index. Data are from Cappi et al. 1997 (0836+710), Singh et al. 1990 (1510−089), and Kubo et al. 1998 (2230+114).

[d] EGRET flux above 100 MeV and energy index. Average of available detections. Data are from Hartman et al. 1999.

*0836+710.*—This is a distant bright FSRQ. VLBI observations show a compact core and ejections of components with superluminal motion, possibly connected to $\gamma$-ray flares (Otterbein et al. 1998).

In the X-ray band 0836+710 has been observed by *ROSAT* and *ASCA* (Cappi et al. 1997). In both cases it showed a flat spectrum that, together with the steep $\gamma$-ray emission, seems to indicate (as data are not simultaneous) that the IC peak lies in the soft $\gamma$-ray band. A deficit of soft photons ($E < 1$ keV) was interpreted as evidence of absorption higher than the Galactic one. Moreover, from a comparison of *ROSAT* and *ASCA* data (Cappi et al. 1997) this absorption appeared to change by $\Delta N_{\rm H} \sim 8 \times 10^{20}$ cm$^{-2}$ on a timescale of less than 2.6 yr (0.8 yr in the quasar frame).

Recently Malizia et al. (2000) reported the detection of 0836+710 by BATSE in the energy range 20–100 keV with a flat spectrum ($\alpha = 0.1$–$0.3$).

The optical spectrum shows broad emission lines superimposed to a broad blue bump continuum, well fitted by a blackbody at a temperature $T \simeq 2.5 \times 10^4$ K and a luminosity $L \simeq 10^{47}$ ergs s$^{-1}$ (Lawrence et al. 1996).

*1510−089.*—It is a nearby highly polarized quasar (HPQ), which presents strong similarities with 3C 273. In particular, it shows a pronounced UV bump (Pian & Treves 1993).

1510−089 has been extensively observed in X-rays by *EXOSAT* (Singh, Rao, & Vaia 1990; Sambruna et al. 1994), *Ginga* (Lawson & Turner 1997), *ROSAT* (Siebert et al. 1996), and *ASCA* (Singh, Shrader, & George 1997). The X-ray spectrum is very flat in the 2–10 keV band, while in the *ROSAT* band it is steeper, suggesting the possible presence of a spectral break around 1–2 keV. The *EXOSAT* observation (Singh et al. 1990) showed the presence of a relatively strong iron line (EW $\simeq$ 800 eV), not detected in more recent observations with *Ginga* and *ASCA*.

*2230+114.*—This quasar has been observed several times with *Ginga* (Lawson & Turner 1997), *ROSAT* (Brinkmann, Siebert, & Boller 1994), and *ASCA* (Kubo et al. 1998). It shows a flat spectrum that extends smoothly into the soft $\gamma$-ray band, as indicated by the OSSE data (McNaron-Brown et al. 1995).

Radio observations reveal a rather complicated structure (see Altschuler et al. 1995, and references therein) and superluminal components. Kellermann et al. (1962) classify 2230+114 as a classical gigahertz-peaked source (e.g., O'Dea 1998).

Falomo, Scarpa, & Bersanelli (1994) report the optical spectrum, which shows bright emission lines superimposed to a blue continuum, typical of a quasar blue bump.

## 3. *BeppoSAX* OBSERVATIONS AND DATA ANALYSIS

The scientific payload of the Italian-Dutch X-ray satellite *BeppoSAX*[12] (see Boella et al. 1997) consists of four coaligned Narrow Field Instruments (NFIs) and two Wide Field Cameras. Two of the NFIs use concentrators to focalize X-rays: the Low Energy Concentrator Spectrometer (LECS) has a detector sensitive to soft–medium X-ray photons (0.1–10 keV), while the Medium Concentrator Spectrometer (MECS) reveals photons in the energy range 1.3–10 keV. The Phoswich Detector System (PDS), sensitive from 12 up to 200 keV, consisting of four identical units, uses rocking collimators so as to monitor source and background simultaneously with interchangeable units. We will not consider here the fourth NFI, a High Pressure Gas Scintillation Proportional Counter (HPGSPC).

The *BeppoSAX* journal of observations is reported in Table 2, with exposure times and observed count rates. The observation of 2230+114 consisted of five short pointings, separated by 1–2 days, while the others were continuous apart from gaps due to satellite constraints. None of the sources showed significant flux variations within the observations. We therefore obtained a cumulative spectrum for each source.

We analyzed the *BeppoSAX* spectral data using the standard software packages XSELECT (version 1.4) and XSPEC (version 10.0) and the 1997 September version of the calibration files released by the *BeppoSAX* Scientific Data Center (SDC). From the event files we extracted the LECS and MECS spectra in circular regions centered around the source with radii of 8′ and 4′, respectively (see the *SAX* Analysis Cookbook[13]). The PDS spectra extracted with the standard pipeline with the rise-time correction were directly provided by the *BeppoSAX* SDC. We used PDS data rebinned with S/N > 3.

For the spectral analysis we considered the LECS data in the restricted energy range 0.1–4 keV, because of unsolved calibration problems at higher energies. Background spectra extracted from blank-field observations at the same position as the source were used. We fitted rebinned LECS, MECS, and PDS spectra jointly, allowing for two variable different normalization factors to take into account uncertainties in the intercalibration of different instruments (see *SAX* Cookbook).

In the following subsections we report the analysis procedure for each object. The results of the spectral fits are summarized in Table 3.

[12] http://www.sdc.asi.it.

[13] ftp://www.sdc.asi.it/pub/sax/doc/software_docs/saxabc_v1.2.ps.gz.

TABLE 2

*BeppoSAX* DATA OBSERVATION LOG

| | | | | LECS | | MECS | | PDS | |
|---|---|---|---|---|---|---|---|---|---|
| SOURCE | DATE | START | END | Exposure (s) | net counts s$^{-1}$ [a] | Exposure (s) | net counts s$^{-1}$ [b] | Exposure (s) | net counts s$^{-1}$ |
| 0836+710 ..... | 1998 May 27–28 | 08:17:47 | 08:13:14 | 18209 | 0.111 ± 0.003 | 42640 | 0.269 ± 0.003 | 16493 | 0.70 ± 0.05 |
| 1510−089 ..... | 1998 Aug 3–4 | 14:23:13 | 14:17:16 | 15880 | 0.025 ± 0.002 | 43870 | 0.056 ± 0.001 | 19371 | 0.31 ± 0.05 |
| 2230+114[c] ..... | 1997 Nov 11–21 | 2:12:24 | 22:51:34 | 50178 | 0.033 ± 0.001 | 103400 | 0.065 ± 0.008 | 47834 | 0.14 ± 0.03 |

[a] 0.1–4 keV.

[b] 1.8–10.5 keV, 2 MECS units.

[c] Total of five pointings.

TABLE 3

FITS TO *BeppoSAX* DATA (LECS + MECS + PDS)[a]

| $\Gamma$[b] | $E_b$[c] (keV) | $\Gamma_h$[c] | $N_H$ ($\times 10^{20}$ cm$^{-2}$) | $F_{[2-10keV]}$ ($\times 10^{-12}$ ergs cm$^{-2}$ s$^{-1}$) | $\chi^2$/dof |
|---|---|---|---|---|---|
| | | | 0836+710 | | |
| $1.33 \pm 0.04$..... | ... | ... | $8.3^{+4.7}_{-2.6}$ | 26 | 63.0/63 |
| $0.8^{+0.4}_{-0.5}$ ..... | $1.2 \pm 0.3$ | $1.31 \pm 0.03$ | 2.83 (fixed) | 26 | 63.1/62 |
| | | | 1510−089 | | |
| $1.43 \pm 0.05$..... | ... | ... | 7.8 (fixed) | 5.2 | 56.55/65 |
| $2.65^{+0.63}_{-0.60}$ ..... | $1.3 \pm 0.3$ | $1.39 \pm 0.08$ | 7.8 (fixed) | 5.3 | 43.1/63 |
| | | | 2230+114 | | |
| $1.51 \pm 0.04$..... | ... | ... | $7.3^{+3.8}_{-2.7}$ | 6.0 | 51.1/51 |
| $0.69^{+0.12}_{-0.08}$ ..... | $0.8^{+0.4}_{-0.3}$ | $1.51 \pm 0.04$ | 5.04 (fixed) | 6.1 | 48.0/50 |

[a] First line single power-law, second line broken power-law model. Errors are quoted at the 90% confidence level for one parameter of interest ($\Delta\chi^2 = 2.71$).

[b] Photon index, related to the spectral index by $\alpha = \Gamma - 1$.

[c] Break energy and high-energy photon index for the broken power-law model.

### 3.1. *0836+710*

The total LECS + MECS + PDS spectrum of 0836+710 is well described by a single absorbed power-law model, with a column density higher than the Galactic value at the 99% confidence level (see Figs. 1 and 2). Assuming a model with fixed Galactic absorption plus a free absorption at the redshift of the source (the ZWABS model of XSPEC) we found that the required intrinsic column density is $N_H = 6.6(2.5\text{–}12.6) \times 10^{21}$ cm$^{-2}$ to the quasar rest frame.

An alternative possibility is to model the spectrum with a broken power law. This gives an extremely flat low-energy slope, with an acceptance probability equivalent to the single power-law plus free absorption model. These results agree well with the findings of Cappi et al. (1997) from *ASCA* data even at different flux levels (see the discussion in § 3.1.1).

The residuals of the fits (see Fig. 1) show an excess around 2 keV in the LECS data. This is just the expected energy of the redshifted fluorescence Fe line at 6.4 keV. Fixing the continuum parameters to the value given by the fit of LECS, MECS, and PDS data for a single power law we tried to model the excess with an unresolved Gaussian line with the energy as a free parameter. The fit converges to the right energy ($E = 2.0 \pm 0.1$ keV, EW $\simeq$ 110 eV), but the improvement in the $\chi^2$ is only marginal (the $F$-test gives a probability $P \sim 90\%$). No excess is present in the MECS spectra at the same energy, which however is near the low-energy end of the MECS sensitivity band, fixed at 1.8 keV (as indicated in the *SAX* Cookbook). We checked whether the feature could be due to extraction problems or contamination: indeed, when extracting the LECS spectrum in a

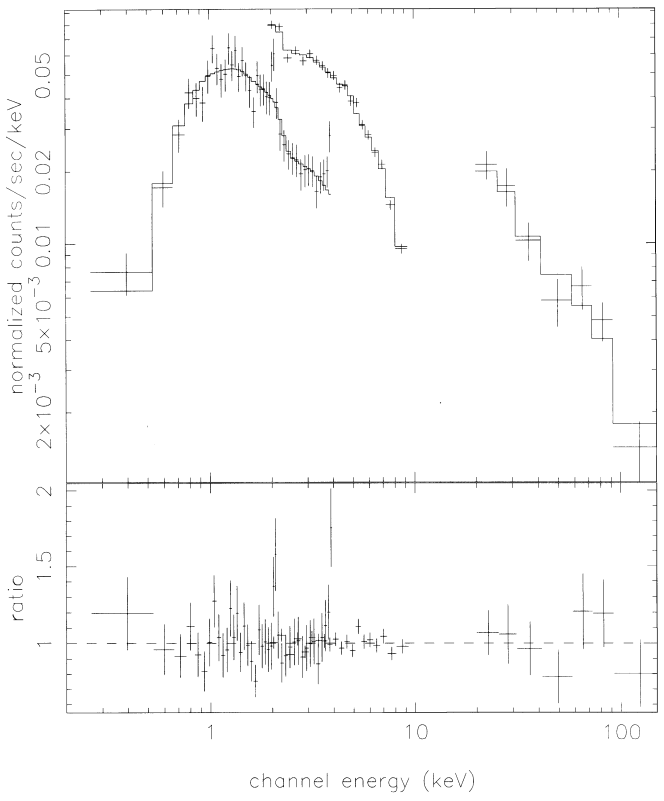


FIG. 1.—Fit with a power law and free absorption for 0836+710

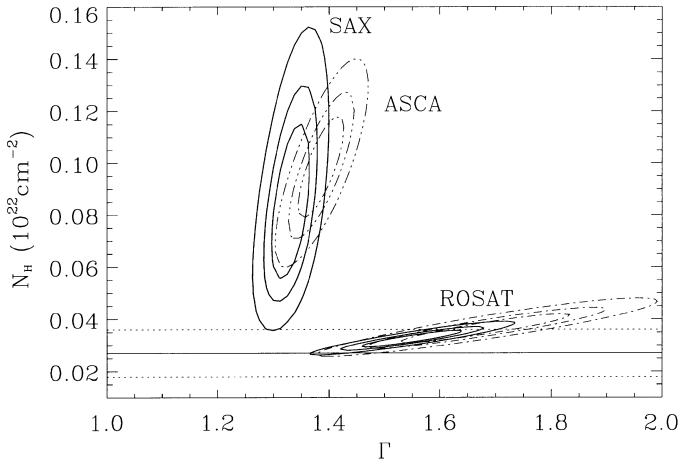


FIG. 2.—68%, 90%, and 99% photon index–$N_H$ confidence contours for *BeppoSAX*, *ASCA*, and *ROSAT* observations of 0836+710. The horizontal solid line indicates the value of the Galactic absorption, and dashed lines indicate the uncertainty range. *BeppoSAX* and *ASCA* data clearly require extra-absorption, while *ROSAT* data are consistent with a steeper, not extra-absorbed spectrum.

smaller region of 4′ the residuals are less evident. We conclude that the emission feature is probably not real.

#### 3.1.1. *Comparison with ROSAT Observations*

In Figure 2 we report the $N_H$ photon index confidence contours of *ROSAT*, *ASCA*, and *BeppoSAX* observations, while in Figure 3 we show the absorption column obtained from different observations as a function of the 0.1–2 keV flux. As noted above, the *BeppoSAX* and *ASCA* confidence contours in Figure 2 are clearly consistent, implying an $N_H$ higher than Galactic and a very flat continuum ($\alpha \sim 0.3$) although the flux during the *BeppoSAX* observation was larger than that measured by *ASCA* by a factor of 2. On the contrary, the *ROSAT* data indicate a steeper spectrum ($\alpha \sim 0.5$) and do not require extra-absorption. In fact, comparing the *ROSAT* and *ASCA* results, Cappi et al. (1997) concluded that the intrinsic absorption had varied between the two observations. Given the consistency of the *ASCA* and *BeppoSAX* results at different flux levels we believe that the discrepancies with the *ROSAT* results may be more plausibly explained by calibration problems of *ROSAT* (see, e.g., Iwasawa, Fabian, & Nandra 1999).

### 3.2. *1510−089*

A fit over the whole range (LECS + MECS + PDS) with a single absorbed power-law model, although statistically acceptable, produces evident excess residuals at low energies and in the PDS band (see Fig. 4, *upper panel*). Using a broken power-law model, with the low-energy photon index steeper than the high-energy one, we obtain a better fit and the low-energy residuals disappear (Fig. 4, *lower panel*). The significant improvement is confirmed by the *F*-test (probability >99.9%). Moreover, this model is consistent with both *ROSAT* and *ASCA* observations described in § 1, which show a large difference in the hard and soft spectral indices. The data are also consistent with a fit with a power-law + blackbody model, the latter having a temperature $kT \simeq 0.2$ keV ($\chi^2 = 39.2$, 56 degrees of freedom (dof). It is interesting to note here that a similar soft excess has been detected in 3C 273 by *EXOSAT*, *ROSAT*, and *BeppoSAX* (Turner et al. 1990; Leach, McHardy, & Papadakis 1995; Laor et al. 1994; Grandi et al. 1997; but see Haardt et al. 1998).

The fit of the three data sets (LECS + MECS + PDS) with a broken power law and free intercalibration factors still gives an unacceptable value of the PDS/MECS normalization: the best-fit value is 1.84, with a 90% level confidence range of 1.3–2.5, while the usual value for the PDS/MECS relative normalization is 0.85 (90% level confidence range of 0.77–0.93; see *SAX* Cookbook). If we fix the normalization to 0.85, the PDS data fall well above the MECS extrapolation (see Fig. 4). The reason for this discrepancy is possibly the contamination by another source that lies in the PDS field of view (we remind the reader that the PDS field of view [FOV] is quite large, ∼1°). The *ROSAT* image centered on 1510−089 shows a very

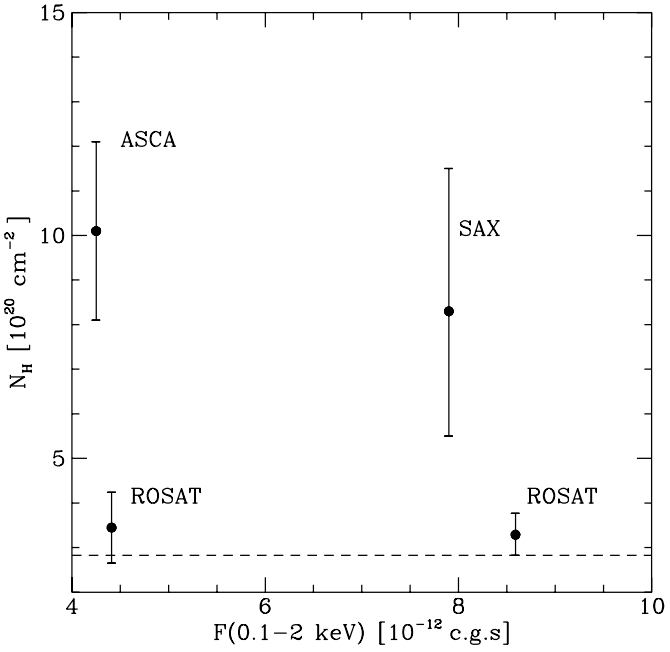


FIG. 3.—$N_H$ (as measured in the observer frame) vs. flux (0.1–2 keV) for different observations of 0836 + 710. The dashed line indicates the Galactic absorption column. *ROSAT* observations are consistent with no extra-absorption, while *ASCA* and *BeppoSAX* observations require intrinsic absorption. No $N_H$-flux correlation seems to be present.

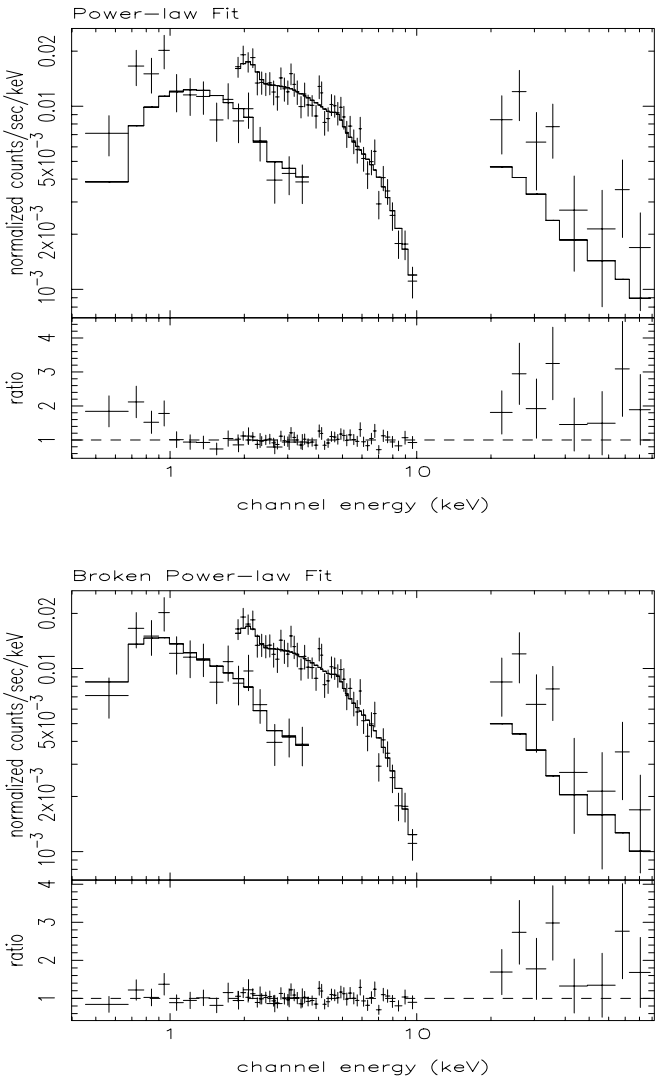


FIG. 4.—Fit of the 1510−089 spectrum (*top*) with a power law and (*bottom*) with a broken power law. The PDS/MECS normalization is fixed to 0.85 in both fits, and the PDS data are clearly in excess to the model (see the discussion in the text).

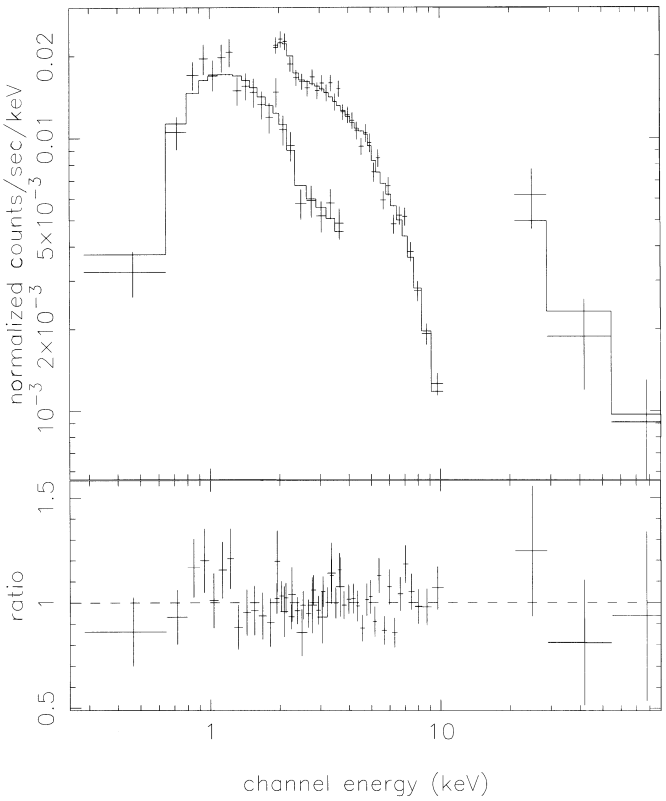


FIG. 5.—Fit with a power law and free absorption for 2230+114

crowded field, and in a radius of 40′ we found six to seven sources with a *ROSAT* flux of 1/10 of the flux of 1510−089. In fact, it is possible that 1510−089 lies in a poor cluster (see, e.g., Yee & Ellingson 1993). The integrated flux from these sources in the *ROSAT* band is $\sim\frac{2}{3}$ of the flux from our target. Since PKS 1510−089 is intrinsically quite hard ($\alpha \simeq 0.4$ in the MECS range) and taking into account that the PDS effective area off-axis is on average $\frac{1}{2}$ of the on-axis area, this source complex cannot contribute significantly in the hard band if it has an average spectral slope $\alpha \simeq 1$. However, it is possible that one of these or other sources may be strongly obscured in the soft–medium X-ray band, giving rise to a significant contribution in the PDS band

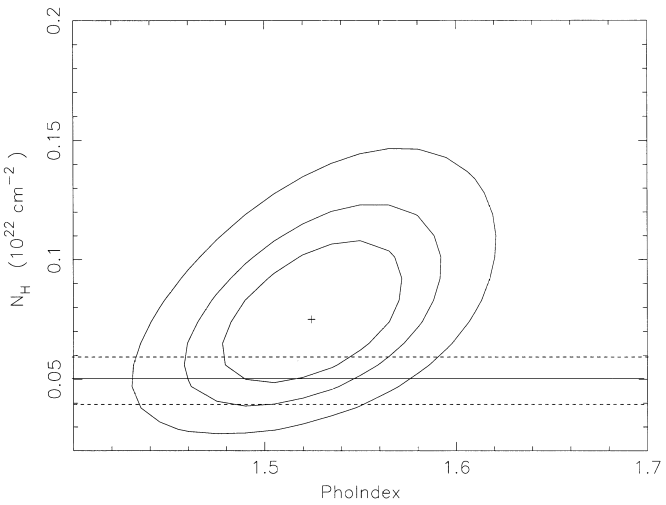


FIG. 6.—68%, 90%, and 99% confidence levels for $N_H$ and spectral index for 2230+114. The solid line indicates the value of the Galactic absorption, while the dashed lines indicate the error range.

despite its weakness in the *ROSAT* field. Therefore, we cannot exclude that the PDS excess is due to contamination from another object, although we are not able to identify it.

Using *EXOSAT* data Singh et al. (1990) found the presence of a relatively strong fluorescence Fe K$\alpha$ line (EW = 800 ± 400 eV), confirmed by Sambruna et al. (1994). The residuals in Figure 4 do not show evidence of this line: fixing the parameters of the continuum and the energy of the line and using a Gaussian profile we found an upper limit to the intrinsic EW of 80 eV, well below the value given by the *EXOSAT* data, which refer to a similar intensity state. Interestingly, this upper limit is consistent with that found in 3C 273 by Grandi et al. 1997 (but see Haardt et al. 1998).

### 3.3. *2230+114*

For 2230+114 we obtain a good fit of the LECS+MECS+PDS spectra with a flat absorbed power-law model (see Fig. 5). There is no evidence for spectral breaks or steepening, and the absorption column is consistent (within 1 $\sigma$) with the Galactic value (see Fig. 6). The residuals do not show evidence of spectral features.

## 4. INTERPRETATION

Using *BeppoSAX* X-ray and quasi-simultaneous optical data and historical data taken from the literature we have assembled the SED shown in Figures 7, 8, and 9 (see the figure legends for the references to the data). In each case the $\gamma$-ray points are averages over the available observations as given in the Third EGRET catalog (Hartman et al. 1999). For the case of 2230+114 the available OSSE and Compton Telescope data are not shown since they partly overlap with the more accurate and simultaneous data from the PDS. The simultaneous optical data were taken at the Torino Observatory with the 1.05 m REOSC telescope.

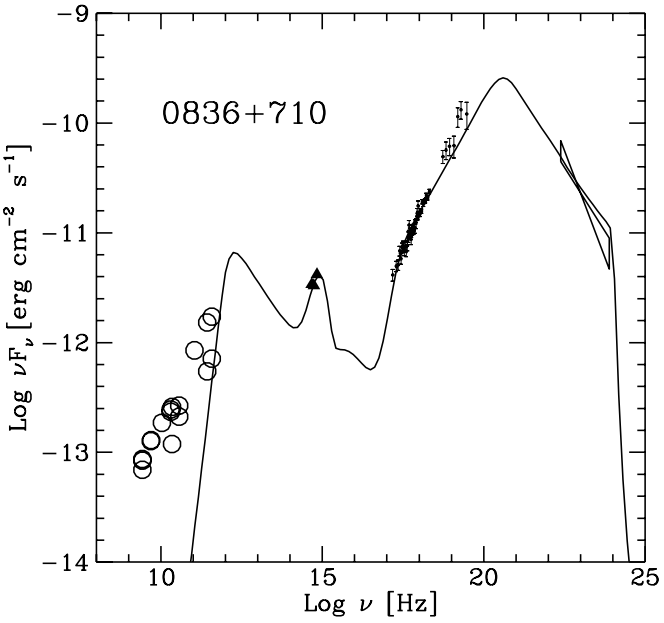


FIG. 7.—Overall SED of 0836+710 with the spectrum calculated using the homogeneous EC model (see text). Circles are historical data taken from Kuhr et al. (1981), Wall & Peacock (1985), Impey & Tapia (1990), Wiren et al. (1992), Edelson (1994; radio), Bloom et al. (1994; far-IR), and Hartman et al. (1999; $\gamma$). Triangles are simultaneous optical data taken at the Torino Observatory. The bump in the model at $\sim 10^{15}$ Hz is due to the blackbody component used to represent the external radiation field.

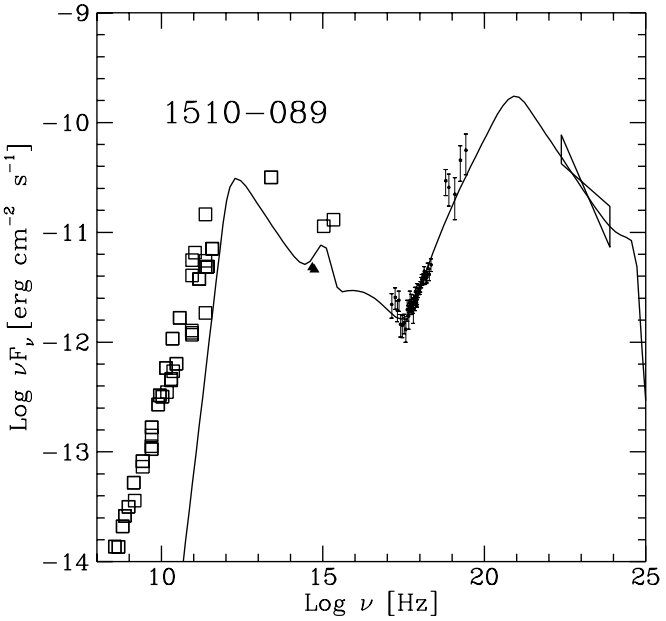


FIG. 8.—Overall SED of 1510−089 with the spectrum calculated using the homogeneous EC model (see text). Data are from Gear et al. (1994), Tornikoski et al. (1996), Landau et al. (1986; radio), Pian & Treves (1993; UV) and Hartman et al. (1999; EGRET). The bump around $10^{16}$–$10^{17}$ Hz is due to the SSC component.

Magnitude calibration was performed according to the photometric sequences in Villata et al. (1997) and Raiteri et al. (1998).

The X-ray data clearly trace the low-energy branch of the high-energy component, whose peak frequency falls above 1 MeV, as estimated using the EGRET data (although the EGRET data are not simultaneous with our X-ray data). Note that the position of the synchrotron peak is very uncertain, because of the poor coverage in the IR band.

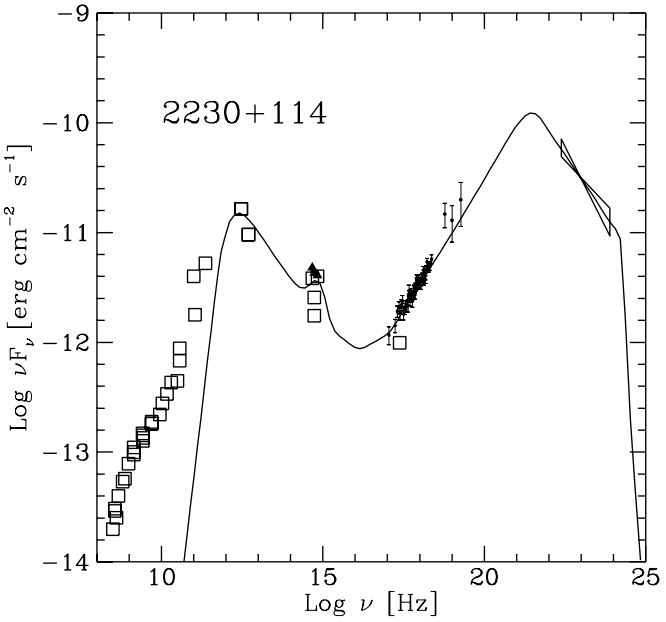


FIG. 9.—Overall SED of 2230+114 with the spectrum calculated using the homogeneous EC model (see text). Data are taken from Kuhr et al. (1981), Wiren at al. (1992), Tornikoski et al. (1996; radio), Impey & Neugebauer (1988; IR), Netzer et al. (1996; optical) and Hartman et al. (1999; EGRET).

Currently the broadband properties of quasar-like blazars are understood in the framework of the EC models. As suggested by the strong thermal features present in the optical-UV spectra (e.g., the blue bump, bright emission lines), the quasar environment is rich in soft photons, produced by the accretion disk and/or by the BLR. In these conditions, in the frame of the emitting source, the energy density of the external soft radiation $U'_{\rm ext}$ can be much higher than the energy density of the synchrotron radiation, and therefore the EC emission can dominate over the SSC emission.

The simplest scenario to account for the emission assumes a spherical homogeneous source filled by relativistic electrons and is fully specified by nine parameters: the size of the emitting region, the Doppler factor, the magnetic field, the energy density and the frequency $\nu_{\rm ext}$ of the external radiation field, and the parameters of the electron distribution. As indicated by the spectral shape of the IC component, flat in X-rays and steep in $\gamma$-rays, the latter can be approximated by a broken power law, specified by two spectral indices, the break energy and the normalization.

The observed SED in principle can yield six quantities, namely, the synchrotron peak frequency and luminosity, the IC peak frequency and luminosity, and the spectral indices of the IC component (directly connected to the indices of the electron distribution). It is worth anticipating that for these blazars the observed peak corresponds to the synchrotron self-absorption frequency of the synchrotron component, which is higher than the peak frequency corresponding to the unabsorbed spectrum.

In addition to these six quantities the typical variability timescale can give an indication of the size of the source. Also in specific sources (e.g., 0836+710) it is possible to have information on the luminosity and the typical frequency of the external radiation field. If the size of the region where this radiation is diluted can be estimated (e.g., with the $R_{\rm BLR}$-$L_{\rm BLR}$ relation for radio-quiet quasars; e.g., Kaspi et al. 2000), the total number of observational constraints (6 + 3) is equal to the number of parameters of the model that can therefore *in principle* be *strongly constrained.*

### 4.1. *Spectral Fits*

In order to reproduce the observed SEDs we adopted the model described in Ghisellini et al. (1998): relativistic electrons with a power-law distribution above a minimum energy are continuously injected in a spherical emitting region with radius $R$, with a magnetic field intensity $B$, and moving with bulk Lorentz factor $\Gamma$ (in the following we assume that the observing angle is $\theta \simeq 1/\Gamma$ and therefore $\delta \sim \Gamma$). The injected electron distribution is characterized by the spectral index $n_{\rm inj}$, the minimum Lorentz factor of particles, $\gamma_{\rm min,\,inj}$, and the injected luminosity $L_{\rm inj}$. Electrons cool rapidly through synchrotron and IC losses reaching an equilibrium distribution, which is essentially a broken power law with indices $n_2 = n_{\rm inj} + 1$ above the break at $\gamma_{\rm min,\,inj}$ and $n_1 = 2$ below the break (in the absence of escape, pair production, and Klein-Nishina effects) down to a minimum Lorentz factor $\gamma_{\rm min}$.

The spectrum of the soft external photons is described by a blackbody with $\nu_{\rm ext} \simeq 1$–$2 \times 10^{15}$ Hz and luminosity $L_{\rm BLR}$ diluted in a spherical region with radius $R_{\rm BLR}$. $L_{\rm BLR}$ can be related to the luminosity observed from the disk by $L_{\rm BLR} = fL_{\rm disk}$, where $f$ represents the fraction of disk luminosity reprocessed in the BLR. We do not consider radiation

TABLE 4

PARAMETERS USED FOR THE EMISSION MODEL DESCRIBED IN THE TEXT

| Source | $R$ ($\times 10^{16}$ cm) | $B$ (G) | $\delta$ | $\gamma_{\rm min,\,inj}$ | $n_{\rm inj}$ | $L_{\rm inj}$ ($\times 10^{45}$ ergs s$^{-1}$) | $L_{\rm BLR}$ ($\times 10^{45}$ ergs s$^{-1}$) | $R_{\rm BLR}$ ($\times 10^{18}$ cm) |
|---|---|---|---|---|---|---|---|---|
| 0836+710 ..... | 4 | 5.9 | 18 | 50 | 3.0 | 1.48 | 3.2 | 1.8 |
| 1510−089 ..... | 2 | 3.1 | 18 | 60 | 3.0 | 0.01 | 0.45 | 1.0 |
| 2230+114 ..... | 4 | 3.5 | 16 | 130 | 3.0 | 0.14 | 0.4 | 1.2 |

coming directly from the accretion disk, which at distances involved here ($\sim 10^{17}$ cm) and for $\Gamma = 5$–10 is strongly redshifted.

The parameters required to reproduce the observed SEDs (Figs. 7, 8, and 9) are given in Table 4. It is interesting to note that the luminosity and size of the BLR are consistent with the observed disk luminosity for $f = 10^{-1}$–$10^{-2}$ and a size $R_{\rm BLR}$ of a fraction of 1 pc. The size of the emitting region and the Lorentz factor have been chosen so as to allow variability with a day timescale as often observed in $\gamma$-rays.

In the SED model shown in Figures 7, 8, and 9 the peak of the synchrotron component is determined by self-absorption. Consequently, at low frequencies the model has the standard self-absorbed spectrum with slope 5/2. Additional emission components from regions farther out in the jet are necessary to account for the spectra at lower frequencies, as indeed expected if the flat radio spectra of blazars are due to the superposition of different self-absorbed components from different locations in the jet. The SEDs calculated here refer to the innermost emitting region.

An interesting feature of the EC model is the presence of a spectral break in the soft X-ray continuum, which reflects very sensitively the minimum energy of the scattering electrons: $\nu_{\rm ICB} \simeq \nu_{\rm ext}\Gamma^2\gamma_{\rm min}^2$ (e.g., Sikora et al. 1997). For $\Gamma \simeq 10$ and $\gamma_{\rm min} \simeq 1$, $\nu_{\rm ICB} \simeq 10^{17}\nu_{\rm ext,\,15}$ Hz. For frequencies below $\nu_{\rm ICB}$ only seed photons with $\nu < \nu_{\rm ext}$ are available, so the Compton spectrum will be depleted (flatter) with respect to the spectrum above $\nu_{\rm ICB}$, where the bulk of the seed photons is scattered (Sikora et al. 1997; Ghisellini 1996). The lack of soft X-ray photons observed in 0836+710, previously interpreted as due to the presence of intrinsic absorption (e.g., Cappi et al. 1997), could be due to a curved spectrum produced by this effect (see Fig. 7). Note that the position of this spectral break strongly constrains $\gamma_{\rm min}$ to be $\leq$ a few. This is relevant for the study of the global energy and matter content in jets (e.g., Celotti & Fabian 1993; Celotti, Padovani, & Ghisellini 1997; Sikora & Madejski 2000).

In general the IC spectrum will be the sum of the SSC and EC emission. For 1510−089 the SSC peak lies at energies between the UV and the soft X-ray band, and its presence could account for the observed soft X-ray excess in the soft X-ray band in this source. Alternatively, this excess could be the hard tail of the observed strong UV bump as proposed for 3C 273. While both the above explanations appear plausible, it is also possible that the excess could be produced by IC scattering of external photons by a population of cold electrons as discussed by Begelman et al. (1987; see also Sikora et al. 1997). For the other two sources the SSC contribution lies well below the EC spectrum.

The adopted model predicts a slope close to 0.5 on the low-energy portion of the IC bump, because of radiatively cooled electrons below the minimum injection energy. In particular for 0836+710 the data require a flatter power law. This might be attributed to the fact that electrons escape before cooling and/or that a reacceleration process energizes the cooled particles.

### 4.2. *Energy Transport in Jets*

The estimate of the physical parameters in the emitting region of $\gamma$-loud quasars allows us to calculate the relevant energy densities and corresponding flux along the jet. This was done initially by Celotti & Fabian (1993) and for a larger sample by Celotti et al. (1997). The total transported energy flux can be expressed as

$$L_k = \pi R^2\Gamma^2(U'_B + U'_e + U'_p)\beta c\ , \qquad (1)$$

where $U'_e$, $U'_p$, and $U'_B$ are the rest-frame energy densities of relativistic electrons, protons, and magnetic field, respectively. $U'_e$ can be expressed as $U'_e = n_e\langle\gamma\rangle m_e c^2$, where $n_e$ is the numerical electron density and $\langle\gamma\rangle$ is the average Lorentz factor. Radiation is excluded from $L_k$ since the jet is optically thin.

In a jet composed of an electron/positron plasma $U'_p = 0$, while for a proton/electron plasma with no cold electrons $n_p = n_e$, and if protons are assumed to be cold, $U'_p/U'_e = m_p/(m_e\langle\gamma\rangle)$. In Table 5 we report the energy densities and the energy fluxes estimated from the spectral model.

We report in row 3 of Table 5 the total emitted power, i.e., the observed power integrated over the whole solid angle (e.g., Sikora et al. 1997).

It appears from Table 5 that the magnetic energy density dominates over the energy density of relativistic electrons but not by a large factor; i.e., it is reasonably close to equipartition.

The radiated power is much larger than that carried by relativistic electrons and by the Poynting flux associated with the field in the emission region. It seems then necessary to postulate that the proton component dominates the energy transport or that the jet is structured so that a large Poynting flux is carried outside the emitting region. If the number density of protons were the same as that of electrons, the proton kinetic power would reach values of the

TABLE 5

VALUES OF ENERGY DENSITIES AND JET LUMINOSITIES OBTAINED FROM THE EMISSION MODEL[a]

| Parameter | 0836+710 | 2230+114 | 1510−089 |
|---|---|---|---|
| $U'_e$ (ergs cm$^{-3}$) ..... | 0.20 | 0.06 | 0.17 |
| $U'_B$ (ergs cm$^{-3}$) ..... | 1.10 | 0.55 | 0.38 |
| $P_{\rm rad}$ ($\times 10^{46}$ ergs s$^{-1}$) ..... | 47.9 | 3.5 | 0.3 |
| $L_e$ ($\times 10^{46}$ ergs s$^{-1}$) ..... | 1.00 | 0.23 | 0.18 |
| $L_B$ ($\times 10^{46}$ ergs s$^{-1}$) ..... | 4.3 | 1.6 | 0.3 |
| $L_p$ ($\times 10^{46}$ ergs s$^{-1}$)[b] ..... | 408 | 75 | 29. |
| $L_{\rm disk}$ ($\times 10^{46}$ ergs s$^{-1}$) ..... | 10.0 | 2.00 | 0.50 |

[a] See text for definitions.

[b] Calculated for $n_p = n_e$.

order of $10^{47}$–$10^{48}$ ergs s$^{-1}$. We recall that this estimate is based on the fact that from the observed X-ray emission we can actually constrain the number of low-energy electrons. The proton contribution would however be overestimated if the jet were partly composed of *relativistic* pair plasma. A large component of *cold* pairs is excluded by our data (except possibly for 1510−089), since it would give rise to an excess around 1 keV, which is not observed (e.g., Sikora & Madejski 2000).

The powers transported by these jets are quite large even when the proton component is not included. It is interesting to compare them with those released by the accretion process, which can be estimated directly from the strength of the blue bump that is measured in all three objects. The derived accretion disk luminosities are listed in the last column of Table 5. For 0836+710 we used the luminosity of the blackbody spectrum fit to the data by Lawrence et al. (1996), while for 1510−089 and 2230+114 we estimated $L_{\rm disk}$ from the UV (Pian & Treves 1993) and the optical spectrum (Falomo et al. 1994), respectively. It is remarkable that in each case the disk luminosity is of the same order as that radiated by the associated jet. Note that in the hypothesis $n_p = n_e$ the power transported in the jets would exceed the luminosity emitted by the accretion disks by a large factor.

Let us briefly discuss the above numbers in the context of the Blandford & Znajek (1977) scenario of powering the jet from the black hole spin. In this model the jet power depends on the black hole mass and angular momentum and on the intensity of the magnetic field threading the horizon. Recently the relation between the magnetic field at the innermost stable orbit of the disk and that at the black hole horizon has been discussed in depth by Ghosh & Abramowitz (1997, hereafter GA) and Livio, Ogilvie, & Pringle (1999, hereafter LOP). Using the standard Shakura & Sunyaev (1973) model for the accretion disk GA arrived at the following expression for the extractable power valid for high accretion rates, when the disk is dominated by radiation pressure:

$$L_{\rm BZ} = 2 \times 10^{44} M_8 \, a^2 \text{ ergs s}^{-1} , \quad (2)$$

where $M_8$ is the black hole mass (in units of $10^8 \, M_\odot$) and $a$ is the spin parameter ($a = 1$ for a maximally rotating black hole).

Comparing this expression with the values found above, we conclude that even for maximal values of the accretion rate, spin parameter, and mass ($10^9 \, M_\odot$), the estimated powers are insufficient for at least two objects. If protons are included the discrepancy becomes extremely large. We are therefore led to suggest that the analysis of GA and LOP probably represents a lower limit to the jet powers produced. In fact Krolik (1999) points out the difficulties of a realistic approach to the determination of the magnetic field near the black hole horizon, while Meier (1999) considers the possibility of a magnetic field amplification due to the frame dragging in the ergosphere of a Kerr hole, leading to jet power estimates larger by a factor 100 than those given by GA. Allowing for this uncertainty we introduce a parameter $\xi$ on the right-hand side of equation (2).

Using now the observed disk luminosity we can write

$$L_{\rm disk} \simeq 1.3 \times 10^{46} \dot{m} M_8 \text{ ergs s}^{-1} \quad (3)$$

(where $\dot{m}$ is the accretion rate in Eddington units, $\dot{m} = L/L_{\rm Edd}$), which, combined with equation (2), yields $\xi M_8 =$ 2400, 180, and 15 and $\dot{m}/\xi = 3 \times 10^{-3}$, $8.5 \times 10^{-3}$, and $2.5 \times 10^{-2}$ for the three objects, respectively. Thus, for $\xi = 100$ we get masses in the range $10^7$–$10^9 \, M_\odot$ and critical accretion rates, while for $\xi = 10$ the masses are higher and the accretion rates lower by a factor 10. We conclude that a value of $\xi$ between 10 and 100 is needed.

## 5. SUMMARY AND CONCLUSIONS

We have analyzed the X-ray spectra of three $\gamma$-ray–loud quasars. The main result of our analysis is that for all sources the X-ray continuum in the 2–100 keV energy band is well represented by a very flat ($\alpha = 0.3$–$0.5$) power law, without evidence for spectral steepening at high energies. Moreover, at soft energies 0836+710 shows evidence for either intrinsic absorption or an extremely hard low-energy continuum. In 1510−089 a soft excess is present at $E < 1$ keV; the presence of an Fe line in this object is not confirmed.

By modeling the SEDs of these three sources as synchrotron and inverse Compton emission from a single population of electrons with a broken power-law energy distribution and including external seed photons for the IC process, we estimated the physical parameters in the emission region and the corresponding energy transport along the jets. While the energy densities of relativistic electrons and of the magnetic field are near equipartition, their energy is insufficient to power the observed radiation, implying that either a significant proton component or Poynting flux outside the emission region is the carrier of power.

Even the minimal jet power required by the observed radiation is very high ($10^{45}$–$10^{47}$ ergs s$^{-1}$) and is of the same order as that thermally emitted in the optical-UV bands by the accretion disk. If the Blandford & Znajek model for extraction of rotational energy from the black hole is responsible for powering the jets, the magnetic field at the black hole horizon must be larger than estimated in recent works on this highly complex and controversial issue.

We thank the *BeppoSAX* SDC for providing us with the cleaned data. We are grateful to the anonymous referee and to Roberto Della Ceca for helpful comments. This work was partly supported by the Italian Ministry for University and Research (MURST) under grant Cofin98-02-32 and by the Italian Space Agency (ASI-ARS-98-91).

## REFERENCES

Altschuler, D. R., Gurvits, L. I., Alef, W., Dennison, B., Graham, D., Trotter, A. S., & Carson, J. E. 1995, A&AS, 114, 197
Begelman, M. C., et al. 1987, ApJ, 322, 650
Blandford, R. D., & Znajek, R. L. 1977, MNRAS, 179, 433
Bloom, S. D., Marscher, A. P., Gear, W. K., Teräsranta, H., Valtaoja, E., Aller, H. D., & Aller, M. F. 1994, AJ, 108, 398
Boella, G., Butler, R. C., Perola, G. C., Piro, L., Scarsi, L., & Bleeker, J. A. M. 1997, A&AS, 122, 299
Brinkmann, W., Siebert, J., & Boller, T. 1994, A&A, 281, 355
Cappi, M., Matsuoka, M., Comastri, A., Brinkmann, W., Elvis, M., Palumbo, G. G. C., & Vignali, C. 1997, ApJ, 478, 492
Celotti, A., & Fabian, A. C. 1993, MNRAS, 264, 228
Celotti, A., Padovani, P., & Ghisellini, G. 1997, MNRAS, 286, 415
Comastri, A., Fossati, G., Ghisellini, G., & Molendi, S. 1997, ApJ, 480, 534
Dermer, C. D., & Schlickeiser, R. 1993, ApJ, 416, 458
Dickey, J. M., & Lockman, F. J. 1990, ARA&A, 28, 215
Dondi, L., & Ghisellini, G. 1995, MNRAS, 273, 583
Edelson, R. A. 1994, AJ, 94, 1150

Falomo, R., Scarpa, R., & Bersanelli, M. 1994, ApJS, 93, 125
Fossati, G., Maraschi, L., Celotti, A., Comastri, A., & Ghisellini, G. 1998, MNRAS, 299, 433
Gear, W. K., et al. 1994, MNRAS, 267, 167
Ghisellini, G. 1996, in IAU Symp. 175, Stellar Surface Structure, ed. K. G. Strassmeier & J. L. Linsky (Dordrecht: Kluwer), 413
Ghisellini, G., Celotti, A., Fossati, G., Maraschi, L., & Comastri, A. 1998, MNRAS, 301, 451
Ghosh, P., & Abramowicz, M. A. 1997, MNRAS, 292, 887 (GA)
Grandi, P., et al. 1997, A&A, 325, L17
Haardt, F., et al. 1998, A&A, 340, 35
Hartman, R. C., et al. 1999, ApJS, 123, 79
Impey, C. D., & Neugebauer, G. 1988, AJ, 95, 307
Impey, C. D., & Tapia, S. 1990, ApJ, 354, 124
Iwasawa, K., Fabian, A. C., & Nandra, K. 1999, MNRAS, 307, 611
Kaspi, S., Smith, P. S., Netzer, H., Maoz, D., Jannuzi, B. T., & Giveon, U. 2000, ApJ, 533, 631
Kellermann, K. I., Long, R. J., Allen, L. R., & Moran, J. M. 1962, Nature, 195, 69
Krolik, J. H. 1999, ApJ, 515, L73
Kubo, H., Takahashi, T., Madejski, G., Tashiro, M., Makino, F., Inoue, S., & Takahara, F. 1998, ApJ, 504, 693
Kuhr, H., Pauliny-Toth, I. I. K., Witzel, A., & Schmidt, J. 1981, AJ, 86, 854
Landau, R., et al. 1986, ApJ, 308, 78
Laor, A., Fiore, F., Elvis, M., Wilkes, B. J., & McDowell, J. C. 1994, ApJ, 435, 611
Lawrence, C. R., Zucker, J. R., Readhead, A. C. S., Unwin, S. C., Pearson, T. J., & Xu, W. 1996, ApJS, 107, 541
Lawson, A. J., & Turner, M. J. L. 1997, MNRAS, 288, 920
Leach, C. M., McHardy, I. M., & Papadakis, I. E. 1995, MNRAS, 272, 221
Livio, M., Ogilvie, G. I., & Pringle, J. E. 1999, ApJ, 512, 100
Lockman, F. J., & Savage, B. D. 1995, ApJS, 97, 1
Malizia, A., Bassani, L., Dean, A. J., McCollough, M., Stephen, J. B., Zhang, S. N., & Paciesas,W. S. 2000, ApJ, 531, 642
McNaron-Brown, K., et al. 1995, ApJ, 451, 575
Meier, D. L. 1999, ApJ, 522, 753
Mukherjee, R., et al. 1997, ApJ, 490, 116
Netzer, H., et al. 1996, MNRAS, 279, 429
O'Dea, C. P. 1998, PASP, 110, 493
Otterbein, K., Krichbaum, T. P., Kraus, A., Lobanov, A. P., Witzel, A., Wagner, S. J., & Zensus, J. A. 1998, A&A, 334, 489
Pian, E., & Treves, A. 1993, ApJ, 416, 130
Raiteri, C. M., Villata, M., Lanteri, L., Cavallone, M., & Sobrito, G. 1998, A&AS, 130, 495
Sambruna, R. M., Barr, P., Giommi, P., Maraschi, L., Tagliaferri, G., & Treves, A. 1994, ApJS, 95, 371
Shakura, N. I., & Sunyaev, R. A. 1973, A&A, 24, 337
Siebert, J., Brinkmann, W., Morganti, R., Tadhunter, C. N., Danziger, I. J., Fosbury, R. A. E., & Di Serego Alighieri, S. 1996, MNRAS, 279, 1331
Sikora, M., Begelman, M. C., & Rees, M. J. 1994, ApJ, 421, 153
Sikora, M., & Madejski, G. 2000, ApJ, 534, 109
Sikora, M., Madejski, G., Moderski, R., & Poutanen, J. 1997, ApJ, 484, 108
Singh, K. P., Rao, A. R., & Vahia, M. N. 1990, ApJ, 365, 455
Singh, K. P., Shrader, C. R., & George, I. M. 1997, ApJ, 491, 515
Stark, A. A., Gammie, C. F., Wilson, R. W., Bally, J., Linke, R. A., Heiles, C., & Hurwitz, M. 1992, ApJS, 79, 77
Tornikoski, M., et al. 1996, A&AS, 116, 157
Turner, M. J. L., et al. 1990, MNRAS, 244, 310
Villata, M., et al. 1997, A&AS, 121, 119
Wall, J. V., & Peacock, J. A. 1985, MNRAS, 216, 173
Wiren, S., Valtaoja, E., Teräsranta, H., & Kotilainen, J. 1992, AJ, 104, 1009
Yee, H. K. C., & Ellingson, E. 1993, ApJ, 411, 43